International Journal of Research in Science & Engineering
ISSN: 2394-8299
Vol: 02, No. 03, April-May 2022
http://journal.hmjournals.com/index.php/IJRISE
DOI: https://doi.org/10.55529/ijrise.23.48.60

Boosting the Power Conversion efficiency of $CsPb_{0.75}Sn_{0.25}IBr_2$ Alloy-based Perovskite Solar Cell with Charge Transport Layer $Mg:SnO_2$: A Theoretical Study

Asha Chauhan[1*], A K Shrivastav[2], Anjali Oudhia[3]

[1,2]Department of Physics, National Institute of Technology, Raipur, Chhattisgarh, 492010, India*
[3]Department of Physics, Govt. Nagarjuna P.G. Science College, Raipur, Chhattisgarh, 492010, India

Corrossponding Email: [1]ashuchauhan4388@gmail.com*

Received: 05 Febaury 2022 **Accepted:** 20 April 2022 **Published:** 26 May 2022

Abstract: ***The perovskite-based photovoltaic cells are the best way to convert photon radiation into electrical energy. The fundamental focus of this work is to stimulate and boost the power conversion efficiency (PCE) of an alloy-based $CsPb_{0.75}Sn_{0.25}IBr_2$ perovskite solar cell. The simulation was run on SCAPS-1D cell simulator software (ver. 3.3.09). In this current work, a perovskite $CsPb_{0.75}Sn_{0.25}IBr_2$ with the suitable composition of ions coupled with Tin-based electron transport layers (ETLs)-SnO_2 and $Mg:SnO_2$. The thickness and defect density of absorber layer-$CsPb_{0.75}Sn_{0.25}IBr_2$ has been optimized. The impact of the thickness variation of ETL-SnO_2 and $Mg:SnO_2$ on device performances was also studied. The effect of working temperature, rate of charge carrier generation, and recombination on photovoltaic outputs like open-circuit voltage (Voc), short-circuit current (Jsc), fill factor (FF), and PCE has been studied and analyzed. The simulated cell achieved an efficiency of 13.82% under optimum conditions. The optimized efficiency was comparatively higher than the experimental efficiency of 11.85%. This study demonstrates the role of optimization of various properties of different layers of solar cells.***

Keywords: SCAPS-1D; $Mg:SnO_2$; Perovskite; $CsPb_{0.75}Sn_{0.25}IBr_2$.

1. INTRODUCTION

In 1954, photovoltaic technology was born in the United State and the first silicon (Si) based solar cell was demonstrated in Bell laboratories with an efficiency of 4%[1]. Since the researchers knew that the efficiency of 4% can't feed the hunger for electrical energy, they were seeking alternative materials with higher PCE and

International Journal of Research in Science & Engineering
ISSN: 2394-8299
Vol: 02, No. 03, April-May 2022
http://journal.hmjournals.com/index.php/IJRISE
DOI: https://doi.org/10.55529/ijrise.23.48.60

stability. The search for new material came with CdTe, CdS, and CIS-based second-generation solar cells [2-3]. But, thanks to intense and seminal scientific works, which pushed the perovskite solar cells (PSCs) to become a new photovoltaic technology with a certified efficiency of >21% in 2019 from 3.8% in 2009 [4]. Hybrid organic-inorganic metal halide perovskites of crystal structure AMX_3, (where A is a cation, M is Pb^{2+}, Sn^{2+}, and X is Cl^-, Br^-, I^- etc.) like-$MAPbI_3$ sandwiched as an absorber layer with NiO and SnO_2 nanorods showed PCE >18% [5]. However, the organic and organic-inorganic-based PSCs suffer a lot from oxygen and moisture present in the external environment [6]. The alternative inorganic cation like Cs, Ca, Sr, etc. can migrate this problem.

Organic ions like Cs^+ based perovskite material have gained the attention of experimenters due to their excellent thermal stability and superior intrinsic property in the external environment. By band engineering, all-inorganic cesium-based PSCs achieved PCE >10% at higher temperatures [7]. Cesium lead halide PSC showed an efficiency of 4.8%, and although the PCE was smaller than that of the organic one, it possesses excellent photostability with negligible hysteresis [8]. The inorganic $CsSnI_3$ Tin (Sn)-based PSC stabilized by excellent phase change from B-γ-$CsSnI_3$ to an air-stable perovskite derivative Cs_2SnI_6. In the presence of oxygen and moisture the $CsSnI_3$ decompose into CsI and SnI_2, further CsI, SnI_2, and O_2 reacted to stabilize, as a stable phase Cs_2SnI_6 [9] with a PCE of 1%. In 2018 [10] a PSC with a PCE of 6.21% was reported based on $CsPbBr_3$ exhibited excellent durability and outdoor stability. The quantum dots (QDs) PSCs also improve the PCE up to 40%. The certified PCE of 7.86% with Carbon quantum dots (CQDs) at interface $TiO_2/CsPbBr_3$ [11], and 9.43%, 9.72% efficiency with Graphene quantum dots (GQDs) at interface $TiO_2/CsPbBr_3$, suggested that the performance enhancement with the insertion of QDs in PSCs [12]. The hole transport free alloy-based device m-$TiO_2/Cs_{0.91}Rb_{0.09}PbBr_3$/C gave an efficiency of 9.86%, hence it may be concluded that the compositional change in ions can improve the PCE [13]. Nan Li et al. changed the concentration of lead (Pb) and Sn in $CsPb_{1-X}Sn_XIBr_2$ perovskite and observed a higher efficiency of 11.53% [14]. The suitable composition and band engineering affect the PCE of the device, as the voids/pinholes fill with the appropriate ions, hence reducing the recombination at the interface [15]. A Large number of simulation and theoretical articles are published nowadays, as it suggests a novel configuration with zero cost and better performance of the device [16-23].

In this study, we established the fact that the composition of Pb and Sn in PSCs has potential in the field of photovoltaic (PV) technology. Firstly, the experimental performance compared with the simulation result for the better optimization of the simulated device. We have simulated an inorganic perovskite $CsPb_{0.75}Sn_{0.25}IBr_2$ material with Spiro-OMeTAD hole transport layer (HTL) and SnO_2 electron transport layer (ETL) as the experimental configuration via SCAPS-1D software [24]. The reason for choosing alloy-based perovskite $CsPb_{0.75}Sn_{0.25}IBr_2$ is that it has a reduced bandgap than that of pristine $CsPbIBr_2$ perovskite, which was in favor of the higher PCE [14]. Further the charge transport layer Mg:SnO_2 combined with the $CsPb_{0.75}Sn_{0.25}IBr_2$ perovskite. The addition of Mg^{2+} into the precursor of SnO_2 does not affect the lattice and crystallinity of SnO_2 [25] since both Mg^{2+} and Sn^{4+} have a similar atomic radius (67 Å and 71 Å, respectively) [26]. Like the alloy-based absorber layer

International Journal of Research in Science & Engineering
ISSN: 2394-8299
Vol: 02, No. 03, April-May 2022
http://journal.hmjournals.com/index.php/IJRISE
DOI: https://doi.org/10.55529/ijrise.23.48.60

the composite Mg:SnO_2 showed a reduced bandgap than that of SnO_2, also Mg:SnO_2 has a smaller valence band offset (VBO) compared to SnO_2. Some of the published articles reported that in PSCs lowering the value of VBO reduced the recombination of charge carriers at interface ETL/perovskite and push the performance of the device [17, 27]. In addition, the impact of temperature, defect density, thickness variation, charge generation, and recombination rate on device performance was also analyzed in our study.

Cell simulation parameters

Currently, a simulation-based software SCAPS-1D attracts the great attention of researchers, as it allows us to design PSCs with various parameters and working environments [24]. PSCs are composed of a light absorber layer, ETL, HTL, front, and back contact. In this observation, all inorganic Pb and Sn-based perovskite $CsPb_{0.75}Sn_{0.25}IBr_2$ was used as an absorber layer and combined with ETL-SnO_2 and HTL-Spiro-OMeTAD with gold contact (Au) as configuration FTO/Spiro-OMeTAD/$CsPb_{0.75}Sn_{0.25}IBr_2$/$SnO_2$/Au. **Fig. 1** shows (a) device architecture (b) energy band diagram and (c,d) current density (mA/cm^2) Vs voltage (V) and (e) energy level diagram. After that, the absorber layer was combined with ETL Mg:SnO_2. The bandgap of the absorber layer $CsPb_{0.75}Sn_{0.25}IBr_2$; ETL layer SnO_2, Mg:SnO_2, and HTL layer Spiro-OMeTAD was 1.78 eV, 3.5 eV, 2.98 eV, and 3.17 eV, respectively. The various parameters of the light absorber layer and charge transport layers were carefully extracted from the literature [14, 16, 17, 21, 22, 23, 25] and summarized in **Table 1**. Note that all the parameters were carefully selected from the mentioned literature. Both types of thermal velocity (electron and hole) have set the value of 10^7 m/s in the whole simulation. The defect density of the perovskite $CsPb_{0.75}Sn_{0.25}IBr_2$ was set as neutral Gaussian type and the defect density level was in between the highest conduction band and lowest valence band. We have also introduced an interfacial defect in our simulation since the device was not completed without interfacial contact, to consider the electron and hole recombinations at interfaces ETL/perovskite and perovskite/HTL. The interfacial defect of the absorber-$CsPb_{0.75}Sn_{0.25}IBr_2$, ETL-$SnO_2$, Mg:$SnO_2$ and HTL-Spiro-OMeTAD layer was set the value of 1 x 10^{15} cm^{-3} and 1 x 10^{11} cm^{-3}, respectively. We have introduced all the parameters like bandgap; thickness of absorber, ETL and HTL layer; electron affinity; dielectric permittivity; effective density of states; electron and hole mobility; shallow uniform donor and acceptor density; and defects in our whole simulation.

Parameters	**FTO [17]**	**Spiro-OMeTAD [16]**	**$CsPb_{0.75}Sn_{0.25}IBr_2$**	**SnO_2 [21]**	**Mg:SnO_2 [21, 25]**
Thickness (nm)	200	100	400 [14]	100	100
Bandgap (eV)	3.5	3.17	1.78 [14]	3.5	2.98
Permittivity	4.0	2.1	3.40	4.4	4.4
Electron affinity (eV)	9.0	3.0	28	9.0	9.0
CB (1/cm^3)	2.2E+17	2.5E+18	2.2E+18 [17]	2.2E+18	2.2E+18
VB (1/cm^3)	1.8E+17	1.8E+19	1.8E+19 [17]	1.8E+19	1.8E+19

International Journal of Research in Science & Engineering
ISSN: 2394-8299
Vol: 02, No. 03, April-May 2022
http://journal.hmjournals.com/index.php/IJRISE
DOI: https://doi.org/10.55529/ijrise.23.48.60

Electron mobility (cm^2/Vs)	2.0E+01	2E-4	49 [22]	2E+03	2E+03
Hole mobility (cm^2/Vs)	1.0E+01	2E-4	63 [22]	1E+02	1E+02
N_A ($1/cm^3$)	2.0E+17	0	0 [23]	2E+19	2E+19
N_D ($1/cm^3$)	0	1E+20	1E+13 [23]	0	0

Table 1. Shows the parameters of experimental configuration FTO/Spiro-OMeTAD/$CsPb_{0.75}Sn_{0.25}IBr_2$/$SnO_2$/Au [14, 16, 17, 21, 22, 23, 25].

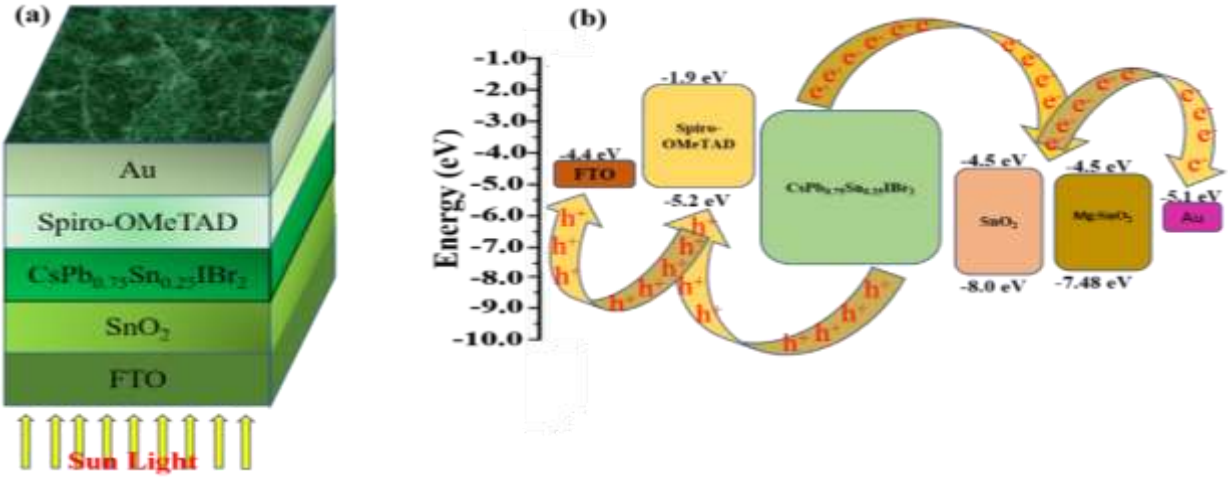

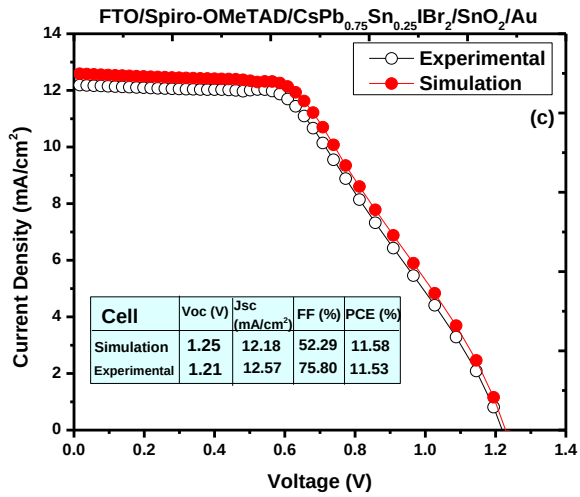

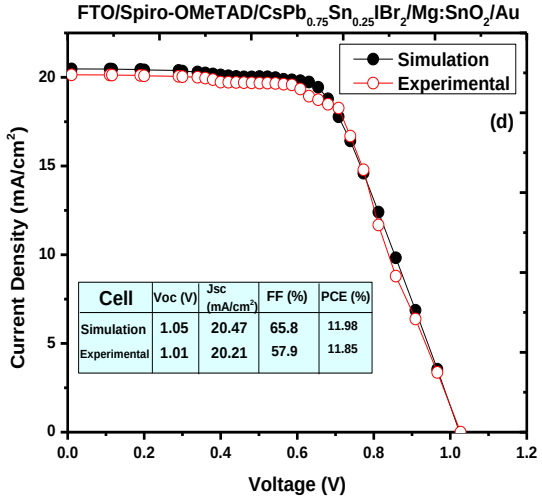

International Journal of Research in Science & Engineering
ISSN: 2394-8299
Vol: 02, No. 03, April-May 2022
http://journal.hmjournals.com/index.php/IJRISE
DOI: https://doi.org/10.55529/ijrise.23.48.60

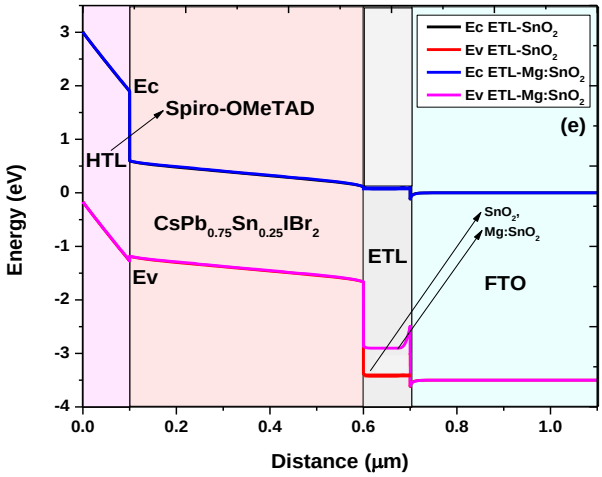

Fig. 1 (a) device architecture (b) energy band diagram and (c, d) current density (mA/cm^2) Vs voltage (V) and (e) energy level diagram [14, 16, 17, 21, 22, 23, 25].

2. RESULT AND DISCUSSION

All the characteristic properties of the simulated device have been studied by using SCAPS-1D software [24] and also compared with reported experimental results. The experimental configuration of FTO/Spiro-OMeTAD/$CsPb_{0.75}Sn_{0.25}IBr_2$/$SnO_2$/Au (PCE 11.53%) and FTO/Spiro-OMeTAD/$CsPb_{0.75}Sn_{0.25}IBr_2$/Mg:$SnO_2$/Au (PCE 11.85%) was in very good agreement with the simulated architecture. The impact of thickness, defect density, and working temperature has been studied and analyzed. In this study, the effect of thickness of the absorber layer was studied and analyzed in six steps from 500 nm to 1000 nm. The performance of 11.58%, 11.54%, 11.50%, 11.42%, 11.30%, and 11.23% was obtained for the thickness of 500 nm, 600 nm, 700 nm, 800 nm, 900 nm, and 1000 nm, respectively for the device FTO/Spiro-OMeTAD/$CsPb_{0.75}Sn_{0.25}IBr_2$/$SnO_2$/Au. On the other hand, Mg-dopped ETL-based device FTO/Spiro-OMeTAD/$CsPb_{0.75}Sn_{0.25}IBr_2$/Mg:$SnO_2$/Au gave an efficiency of 11.85% which was dropped to 11.81% for the thickness 500-1000 nm. In our observation, the optimized thickness of the absorber layer $CsPb_{0.75}Sn_{0.25}IBr_2$ was 500 nm. As the thickness increases resultant, the decrease in performance of the device. The increase in the thickness of the absorber layer caused more absorbance of photons and a higher magnitude of absorbed light enhances the generation of electron-hole pairs, hence improving the PCE, Voc, and Jsc [16, 19, 20]. On the other hand, a thicker absorbing layer also promotes the recombination of electron-hole pairs at the interface which causes the deterioration in PCE [20]. Also, for the higher thickness, the photons are absorbed deep into the absorber layer and increased the diffusion length as a result the charge carrier cannot reach the depletion region leads to the bulk recombination [28]. The efficiency of both configurations for the thickness of 500 nm significantly matched the experimental results [14]. Also, the reduction in the bandgap of Mg-doped SnO_2 and alloy-based absorber $CsPb_{0.75}Sn_{0.25}IBr_2$ was in favor of the simulated FTO/Spiro-OMeTAD/$CsPb_{0.75}Sn_{0.25}IBr_2$/Mg:$SnO_2$/Au device [25]. The PV outputs with the thickness of the absorber layer were shown in **Fig. 2.**

International Journal of Research in Science & Engineering
ISSN: 2394-8299
Vol: 02, No. 03, April-May 2022
http://journal.hmjournals.com/index.php/IJRISE
DOI: https://doi.org/10.55529/ijrise.23.48.60

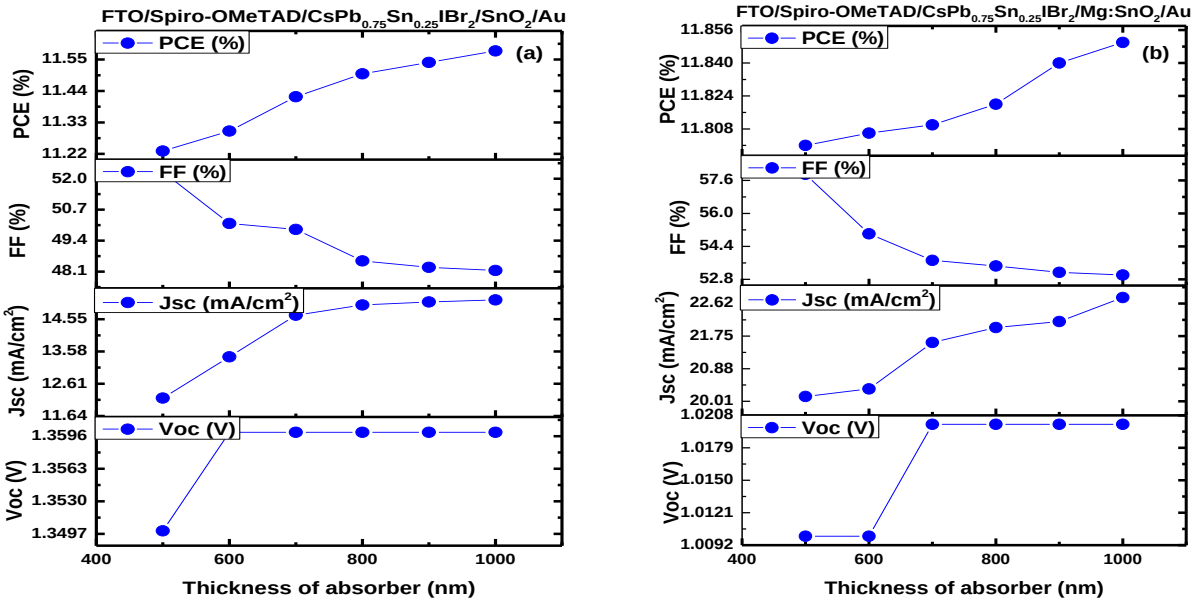

Fig. 2 The variation in the photovoltaic performances with the thickness of the absorber layer for both ETL SnO_2 and Mg: SnO_2-based simulated PSCs.

After optimizing the thickness of the absorber layer, we have also checked the effect of the thickness of ETL layers on the energy cell performances. Since the ETL and HTL layers extract, all the photogenerated electrons and holes from the absorber layer its thickness is also a very important factor while optimizing the device. The ETLs and HTLs layer of PSCs are the two major parts, ETL layer extracts the electrons generated in the absorber layer and sends them towards the respective cathode, while the HTL layer extracts the holes from the absorber layer and transfers it towards the anode [6]. In our simulation, we used Spiro-OMeTAD as HTL and SnO_2 as ETL with the absorber layer. We have also studied the effect of Mg-doped SnO_2 on performance [14, 21, 25]. Mg-doped SnO_2 as ETL has a bandgap of 2.98 eV, which was smaller than pristine SnO_2 and favored in the performances. [25]. The simulated PSC with ETL-Mg:SnO_2 showed an efficiency of 11.85%, which was more than that of SnO_2-based PSC. This observation indicated that a certain amount of additive in the precursor can improve the PCE of the device [15]. The thickness of both ETL and HTL layers varied from 40 nm to 100 nm in four steps. **Fig. 3** showed the variation in performances like Voc, Jsc, FF, and PCE with the thickness of the ETL layer. The optimized thickness of the ETL layer was 40 nm which showed an efficiency of 11.60% and 11.99% for both devices. No large variation was found in PCE, Voc, Jsc, and FF. The ultimately thin ETL layer facilitates the enhanced photogenerated charge transport toward the electrode and introduces dynamic charge transport at the interface of ETL and perovskite [30]. Also, a higher efficiency was observed in Mg: SnO_2-based cells because it has a lower VBO value than that of SnO_2 [17, 27], which reduced the recombination of electron-hole pairs at the interface hence pushing the PCE of the device.

International Journal of Research in Science & Engineering
ISSN: 2394-8299
Vol: 02, No. 03, April-May 2022
http://journal.hmjournals.com/index.php/IJRISE
DOI: https://doi.org/10.55529/ijrise.23.48.60

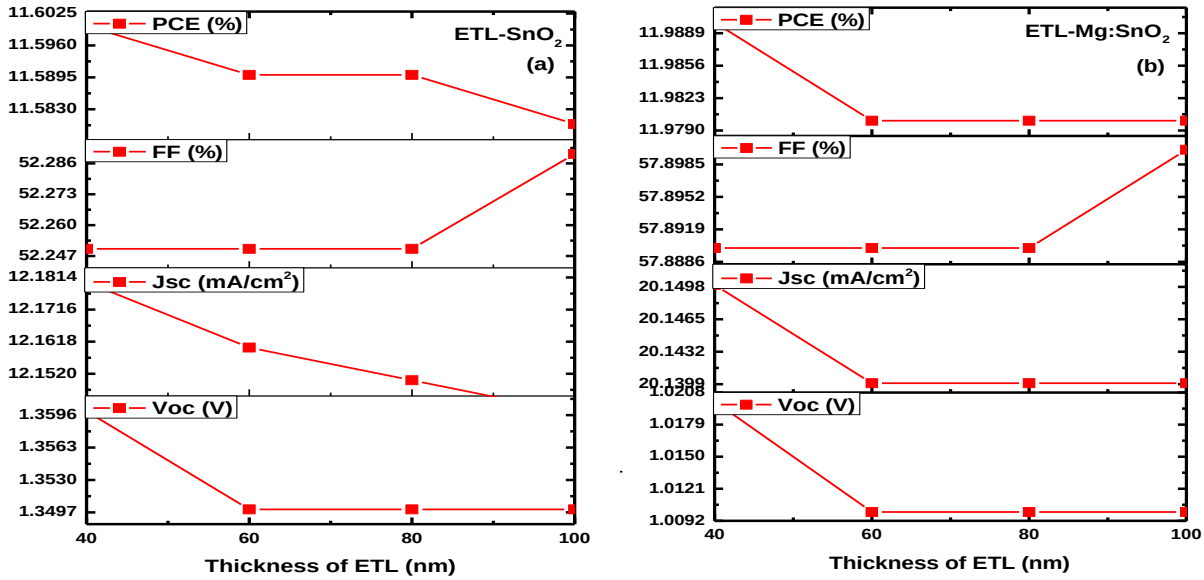

Fig. 3 The effect of thickness of ETL layer on device performance.

We generally test our device under a lab facility, but the solar cell is implanted under the roof of sunlight and various seasons like summer, winter, and rain. So, the effect of outdoor temperature on the cells needs to be tested for stability measurements. The effect of temperature was studied in four steps from 300 K to 500 K as shown in **Fig. 4.** As the temperature increased from 300 K to 500 K a deterioration was observed in Voc from 1.35 V to 1.11 V for a PSC based on SnO_2. While the Voc decreased to 0.89 V for Mg: SnO_2-based device. On the other hand, the Jsc (mA/cm^2) increased to 14.15 mA/cm^2 and 24.73 mA/cm^2 for SnO_2 and Mg:SnO_2 devices, respectively. However, the rate of decrement of all the PV outputs was not the same. The increase in the Jsc value was due to the thermal generation of the charge carrier with a higher working temperature [20]. For both devices, the working temperature of 340 K gave the higher PCE. The rate of carrier generation and total recombination was shown in **Fig. 4.** The highest carrier generation of 1.0E+23 (cm^{-3}s^{-1}) was observed. As reported in published articles, the carrier generation decreased from SnO_2 to Spiro-OMeTAD as the illumination fell on the device [18]. The total recombination rate was less than that of total carrier generation, which was a good indication for PSCs. However, we found that the PSC based on Mg:SnO_2 enhanced the PCE and other photovoltaic performances. The entire observation was in good agreement with the experimental results and previously published articles.

International Journal of Research in Science & Engineering
ISSN: 2394-8299
Vol: 02, No. 03, April-May 2022
http://journal.hmjournals.com/index.php/IJRISE
DOI: https://doi.org/10.55529/ijrise.23.48.60

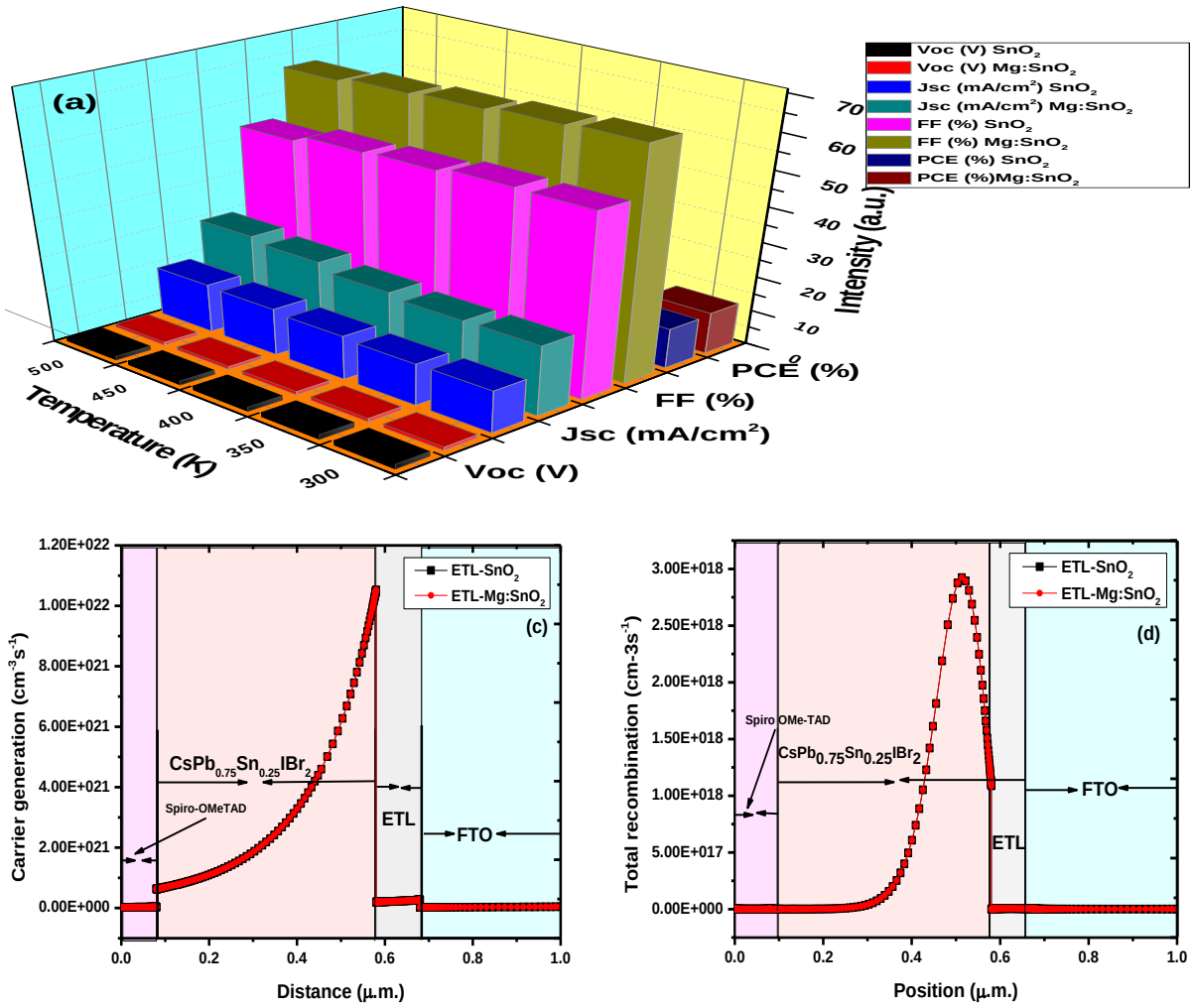

Fig. 4 (a) the impact of temperature on Voc, Jsc, FF, and PCE of the PSCs (c), (d) the carrier generation and total recombination of both devices.

The defect and void/pinhole-free perovskite layer can enhance the performance of the cell significantly, as it doesn't allow the direct contact of ETL/perovskite and perovskite/HTL layers [25]. The effect of defect density was also studied in five steps from 1.0E+11 (cm^{-3}) to 1.0E+15 (cm^{-3}) as shown in **Fig. 5**. The decrement in the performance was observed with the increase in the defect density since the defect contained surface enlarges the recombination at the interface between ETL/perovskite and perovskite/HTL [18], this defect causes the direct linkage of ETL-perovskite and HTL-perovskite. For ETL-SnO_2-based devices, as the defect density increased from 1.0E+11 (cm^{-3}) to 1.0E+15 (cm^{-3}) the performance was decreased to 1.38% from 13.47%, while for ETL-Mg:SnO_2 based devices the PCE decreased to 1.98% from 13.82%. The other parameters like Voc (V), Jsc (mA/cm^2), and FF (%) are also affected by the defect density variation since all the PV performances are very much related to each other's [19]. The absorber layer contains a defect in many forms like vacancies, interstitial, Schottky, and Frenkel defects. The defect can exist at a deep or shallow level in between the energy band which can trap the generated electron and hole pairs, hence reducing the performances [29]. In

International Journal of Research in Science & Engineering
ISSN: 2394-8299
Vol: 02, No. 03, April-May 2022
http://journal.hmjournals.com/index.php/IJRISE
DOI: https://doi.org/10.55529/ijrise.23.48.60

these observations both the ETL layer SnO_2 and Mg:SnO_2 showed a similar variation in the PV performances. From this, we have concluded that the alloy-based PSCs when structured with doped-ETL can improve the performance of the PV cells.

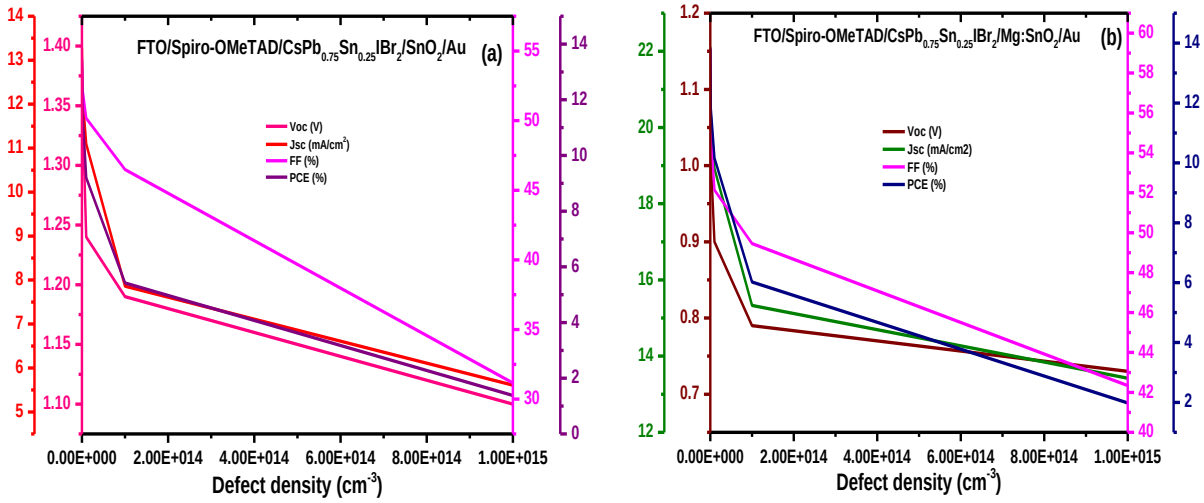

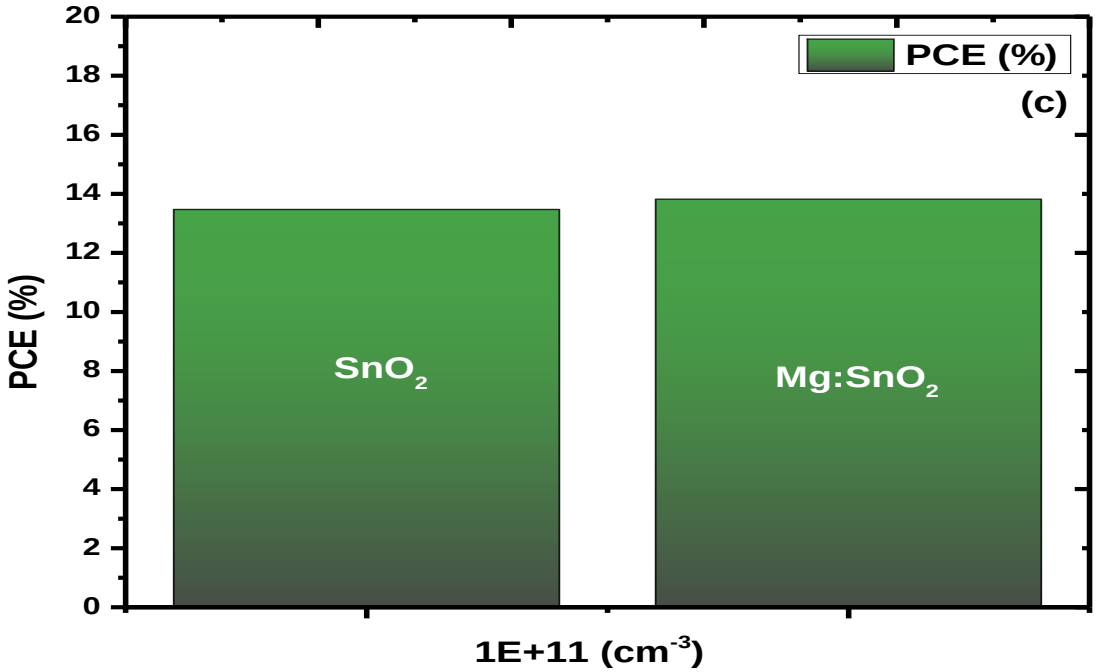

International Journal of Research in Science & Engineering
ISSN: 2394-8299
Vol: 02, No. 03, April-May 2022
http://journal.hmjournals.com/index.php/IJRISE
DOI: https://doi.org/10.55529/ijrise.23.48.60

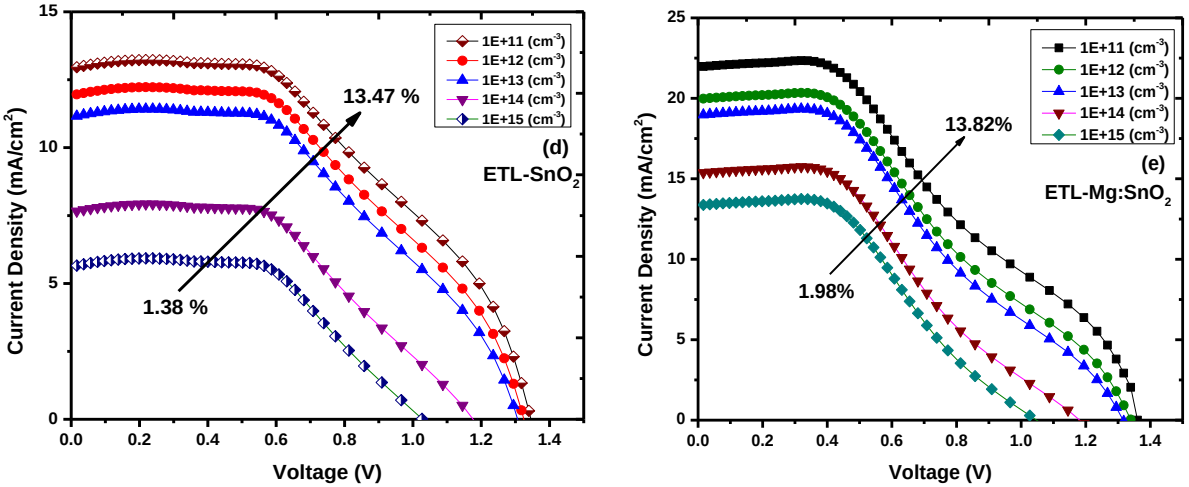

Fig. 5 (a), (b) the variation in PV outputs of SnO_2, Mg:SnO_2 (c) the comparison of PCE of SnO_2 and Mg:SnO_2 (ETL) based device; (d), (e) J-V characteristic with variation in defect density.

3. CONCLUSION

To get high-efficiency inorganic alloy-based perovskite $CsPb_{0.75}Sn_{0.25}IBr_2$ PSC material have simulated via SCAPS-1D with the two charge transport layers SnO_2 and Mg:SnO_2. The perovskite $CsPb_{0.75}Sn_{0.25}IBr_2$ when structured with Mg:SnO_2 (ETL) efficiency was improved up to 13.82% from 11.85%. The impact of the thickness of ETL, HTL, and the absorber layer, defect density, working temperature, carrier generation, and total recombination was studied and analyzed. The optimized thickness of the absorber layer (500 nm) and ETL layer (40 nm), at a working temperature of 340 K, and defect density of 1E+11 (cm^{-3}) showed an improved PCE of 13.82%. Fabricating the PSCs with a thin absorber and ETL layer not only improved the PCE, but it reduces the cost of the device also.

Acknowledgment
The authors would like to thank Professor Marc Burgelman, University of Gent, Department of Electronics and Information System for the development of the SCAPS software package and for allowing its use.

4. REFERENCES

1. The History of Solar; Energy Efficiency and Renewable Energy; U.S. Department of Energy https://www1.eere.energy.gov/solar/pdfs/solar_timeline.pdf.
2. H.D. Pham, T.C-J. Yang, S.M. Jain, G.J. Wilson, and P. Sonar. Development of Dopant-Free Organic Hole Transporting Materials for Perovskite Solar Cells. Adv. Energy Mater., 2020, 1903326, Doi: https://doi.org/10.1002/aenm.201903326.
3. R. G. Lemus and L.E. Shephard. Low-Carbon Energy in Africa and Latin America, Lecture Notes in Energy 38, 2017, 149-173, Doi: https://doi.org/10.1007/978-3-319-52311-8_6.

International Journal of Research in Science & Engineering
ISSN: 2394-8299
Vol: 02, No. 03, April-May 2022
http://journal.hmjournals.com/index.php/IJRISE
DOI: https://doi.org/10.55529/ijrise.23.48.60

4. PEROVSKITE PHOTOVOLTAICS, Basic to Advanced Concepts and Implementation; Publisher: Joe Hayton, (2019), ISBN: 978-0-12-812915-9.
5. Z. Zhu, Y. Bai, X. Liu, C.-C. Chueh, S. Yang, and K.-Y.A. Jen. Enhanced Efficiency and Stability of Inverted Perovskite Solar Cells Using Highly Crystalline SnO_2 Nanocrystals as the Robust electron-transporting Layer. Adv. Mater., 28(30), 2016, 6478-6484, Doi: https://doi.org/10.1002/adma.201600619.
6. Q. Tai, K.-C. Tang, and F. Yan. Recent progress of inorganic perovskite solar cells. Energy Environ. Sci., 12, 2019, 2375, Doi: https://doi.org/10.1039/c9ee01479a.
7. Q. Ye, Y. Zhao, S. Mu, P. Gao, X. Zhang, and J. You. Stabilizing the black phase of cesium lead halide inorganic perovskite for efficient solar cells, Science China Chemistry, 62(7), 2019, 810-821, Doi: https://doi.org/10.1007/s11426-019-9504-x.
8. M. Aamir, T. Adhikari, M. Sher, N. Revaprasadu, W. Khalid, J. Akhtar, and J.-M. Nunzi. Fabrication of planar heterojunction $CsPbBr_2I$ perovskite solar cell using ZnO as electron transport layer & improved solar energy conversion efficiency. J. Name., 00, 1-3, 2013, Doi: https://doi.org/10.1039/x0xx00000x.
9. X. Qiu, B. Cao, S. Yuan, X. Chen, Z. Qiu, Y. Jiang, Q. Ye, H. Wang, H. Zeng, J. Liu, M. G. Kanatzidis. From unstable $CsSnI_3$ to air-stable Cs_2SnI_6: A lead-free perovskite solar cell light absorber with a bandgap of 1.48 eV and high absorption coefficient. Solar Energy Materials & Solar Cells 159, 2017, 227–234, Doi: http://dx.doi.org/10.1016/j.solmat.2016.09.022.
10. Z. Liu, B. Sun, X. Liu, J. Han, H. Ye, T. Shi, Z. Tang, G. Liao. Efficient Carbon-Based $CsPbBr_3$ Inorganic Perovskite Solar Cells by Using Cu-Phthalocyanine as Hole Transport Material. Nano-Micro Lett., 10:34, 2018, Doi: https://doi.org/10.1007/s40820-018-0187-3.
11. J. Ding, Y. Zhao, J. Duan, B. He, and Q. Tang. Alloy-Controlled Work Function for Enhanced Charge Extraction in all-inorganic $CsPbBr_3$ Perovskite Solar Cells. ChemSusChem, 11, 2018, 1432-1437, Doi: http://dx.doi.org/10.1002/cssc.201800060.
12. F. Yang, D. Hirotani, G. Kapil, M.A. Kamarudin, C.H. Ng, Y. Zhang, Q. Shen, and S. Hayase. All-Inorganic $CsPb_{1-x}GexI_2Br$ Perovskite with Enhanced Phase Stability and Photovoltaic Performance. Angewandte Chemie, 57, 39, 2021, 12745-12749, Doi:https://doi.org/10.1002/anie.201807270.
13. Y. Li, J. Duan, H. Yuan, Y. Zhao, B. He, and Q. Tang. Lattice Modulation of Alkali Metal Cations Doped $Cs_{1-x}R_xPbBr_3$ Halides for Inorganic Perovskite Solar Cells. Sol. RRL., 2018, 1800164, Doi: https://doi.org/10.1002/solr.201800164.
14. N. Li, Z. Zhu, J. Li, A.K.-Y. Jen, and L. Wang. Inorganic $CsPb_1$-$xSnxIBr_2$ for Efficient Wide-Bandgap Perovskite Solar Cells. Adv. Energy Mater. 2018, 1800525; Doi: https://doi.org/10.1002/aenm.201800525.
15. M. Cha, P. Da, J. Wang, W. Wang, Z. Chen, F. Xiu, G. Zheng, and Z.-S. Wang. Enhancing Perovskite Solar Cell Performance by Interface Engineering Using $CH_3NH_3PbBr_{0.9}I_{2.1}$ Quantum Dots; J. Am. Chem. Soc., 138, 2016, 8581−8587, Doi: https://doi.org/10.1021/jacs.6b04519.
16. W. Isoe, M. Mageto, C. Maghanga, M. Mwamburi, V. Odari, and C. Awino. Thickness Dependence of Window Layer on $CH_3NH_3PbI_{3-X}Cl_X$ Perovskite Solar Cell. International Journal of Photoenergy Volume, 2020, 8877744, Doi: https://doi.org/10.1155/2020/8877744.

International Journal of Research in Science & Engineering
ISSN: 2394-8299
Vol: 02, No. 03, April-May 2022
http://journal.hmjournals.com/index.php/IJRISE
DOI: https://doi.org/10.55529/ijrise.23.48.60

17. Y. Raoui, H.E. Zahraouy, S. Kazim, and S. Ahmad. Energy level engineering of charge selective contact and halide perovskite by modulating band offset: Mechanistic insights. Journal of Energy Chemistry, 54, 2021, 822–829, Doi: https://doi.org/10.1016/j.jechem.2020.06.030.
18. M. Mehrabian, E. N. Afshar, and S.A. Yousefzadeh. Simulating the thickness effect of the graphene oxide layer in $CsPbBr_3$-based solar cells. Mater. Res. Express, 8, 2021, 035509, Doi: https://doi.org/10.1088/2053-1591/abf080.
19. K. Chakraborty, M.G. Choudhury, and S. Paul. Numerical study of Cs_2TiX_6 ($X=Br^-$, I^-, F^- and Cl^-) based perovskite solar cell using SCAPS-1D device simulation. Solar Energy, 194, 2019, 886–892, Doi: https://doi.org/10.1016/j.solener.2019.11.005.
20. S. Ahmed, F. Jannat, Md. A.K. Khan and M. A. Alim. Numerical development of eco-friendly Cs_2TiBr_6 based perovskite solar cell with all-inorganic charge transport materials via SCAPS-1D. Optik, 20, 2021, 31591, Doi: https://doi.org/10.1016/j.ijleo.2020.165765.
21. P. Roy, S. Tiwari, A. Khare. An investigation of the influence of temperature variation on the performance of tin (Sn) based perovskite solar cells using various transport layers and absorber layers. Results in Optics, 4, 2021, 100083, Doi: https://doi.org/10.1016/j.rio.2021.100083.
22. Y. He, Z. Liu, K.M. McCall, W. Lin, and D.Y. Chung. Perovskite $CsPbBr_3$ single crystal detector for alpha-particle spectroscopy. Nuclear Inst. and Methods in Physics Research A, 922, 2019, 217–221, Doi: https://doi.org/10.1016/j.nima.2019.01.008.
23. G. Tong, T. Chen, H. Li, W. Song, Y. Chang, J. Liu, L. Yu, J. Xu, Y. Qi, and Y. Jiang. High Efficient Hole Extraction and Stable All-Bromide Inorganic Perovskite Solar Cells via Derivative-Phase Gradient Bandgap Architecture. Sol. RRL, 2019, 1900030, Doi: https://doi.org/10.1002/solr.201900030.
24. Marc. Burgelman, Department of Electronics and Information System, University of Gent. SCAPS-1D. https://scaps.elis.ugent.be/.
25. N. Liu, M. Chen, H. Yang, M. Ran, C. Zhang, X. Luo, H. Lu, and Y. Yang. TiO_2/Mg-SnO_2 nanoparticle composite compact layer for enhancing the performance of perovskite solar cells. Optical Materials Express, 10, 1, 2020, Doi: https://doi.org/10.1364/OME.380354.
26. D. Iskenderoglu and H. Guney. Effect of Mg dopant on SnO_2 thin films grown by spray pyrolysis technique; Modern Physics Letters B, 2019, 1950030, Doi: https://doi.org/10.1142/S0217984919500301.
27. T. Minemoto and M. Murata. Theoretical analysis on the effect of band offsets in perovskite solar cells. Solar Energy Materials and Solar Cells, 133, 2015, 8-14, Doi: https://doi.org/10.1016/j.solmat.2014.10.036.
28. B. Saparov, F. Hongs, J.-P. Sun, H.-S. Duan, W. Meng, S. Cameron, L.G. Hill, Y. Yan, and D.B. Mitzi. Thin-Film Preparation and Characterization of $Cs_3Sb_2I_9$: A Lead-Free Layered Perovskite Semiconductor; Chem. Mater., 27(16), 2015, 5622-5632, Doi: https://doi.org/10.1021/acs.chemmater.5b01989.
29. P. K. Patel. Device simulation of highly efficient eco-friendly $CH_3NH_3SnI_3$ perovskite solar cell. Scientific reports; 2011, 11:3082, Doi: https://doi.org/10.1038/s41598-021-82817-w.

International Journal of Research in Science & Engineering
ISSN: 2394-8299
Vol: 02, No. 03, April-May 2022
http://journal.hmjournals.com/index.php/IJRISE
DOI: https://doi.org/10.55529/ijrise.23.48.60

30. N.A.A. Malek, N. Alias, S.K.Md. Saad, N.A. Abdullah, X. Zhang, X. Li, Z. Shi, M.M. Rosli, T.H. T.A. Aziz, A.A. Umar, and Y. Zhan. Ultra-thin MoS_2 nanosheet for electron transport layer of perovskite solar cells. Optical Materials 104, 2020, 109933, Doi: https://doi.org/10.1016/j.optmat.2020.109933.